International Journal of Mechanical Sciences 215 (2022) 106953

Contents lists available at ScienceDirect

International Journal of Mechanical Sciences

journal homepage: www.elsevier.com/locate/ijmecsci

Simultaneously achieving strength and ductility in Ni_3Al nanowires with superlattice intrinsic stacking faults

Zhiwei Zhang [a,b], Qiang Fu [c], Jun Wang [a,*], Rong Yang [a], Pan Xiao [a], Fujiu Ke [d], Chunsheng Lu [e]

[a] State Key Laboratory of Nonlinear Mechanics (LNM), Institute of Mechanics, Chinese Academy of Sciences, Beijing 100190, China
[b] School of Engineering Science, University of Chinese Academy of Sciences, Beijing 100049, China
[c] Aero Engine Academy of China, Beijing 101304, China
[d] School of Physics, Beihang University, Beijing 100191, China
[e] School of Civil and Mechanical Engineering, Curtin University, Perth, WA 6845, Australia

ARTICLE INFO

Keywords:
Ni_3Al
Stacking faults
Strengthening
Ductility
Molecular dynamics

ABSTRACT

Simultaneously improving strength and ductility has been an attractive theme in materials science and engineering. Through designing nanostructures, it is possible to overcome the traditional trade-off between ductility and strength of materials. In this paper, we show that introducing superlattice intrinsic stacking faults in nickel aluminide (Ni_3Al) can facilitate its strength and toughness. In comparison with twin boundaries, the enhancing effect of superlattice intrinsic stacking faults is more obvious. Most significantly, the yield strength of samples with superlattice intrinsic stacking faults is always superior to their single crystalline counterparts, indicating that the yield strength of single crystalline Ni_3Al can be exceeded. These findings provide new insights into the nanostructural design of aerospace materials.

1. Introduction

Nanostructured metallic materials with ultrafine-grained, heterogeneous and even defective structures show exceptional mechanical properties such as superior strength, which are very promising in various applications. However, super-strong metallic nanomaterials usually have a low ductility at ambient temperature, which significantly restricts their wide usage [1]. Nevertheless, several nanostructured metals and alloys have been found to exhibit a concurrent high strength and good ductility, including nanostructured twinning, gradient-structured and heterogeneous lamella materials [2–4] as well as other types of hetero-structured materials [5,6]. It has shown that planar defects of twin boundary (TB) can simultaneously enhance strength and ductility of nanostructured face-centered-cubic (FCC) metallic materials [2,7–9].

Because of low stacking faults energy in FCC metals, there are a large number of stacking faults generated during plastic deformation via slip of partial dislocations or dissociation of full dislocations. Here, it is worth noting that, similar to TBs, stacking faults are a kind of planar defects. However, there is lack of progress on how stacking faults affect strength and ductility of nanostructured FCC metals. This is mainly due to the difficulty of differentiating individual contributions in FCC metals, since formation of stacking faults is accompanied with deformation twins. Therefore, the observed mechanical behaviors are usually attributed to TBs [8,9]. Whereas stacking faults should in no doubt have a positive impact on strength and ductility of nanostructured FCC metals and alloys. For example, stacking faults can effectively increase the strength of FCC structural materials such as Ag and Au [10]. Moreover, the effect of stacking faults on strength and ductility was obviously observed in nanostructured hexagonal close packed metals and alloys [11–13]. As discovered in nanostructured Mg alloy, stacking faults are effective on blocking and accumulating dislocations, which plays a similar role as TBs. Consequently, the high density of stacking faults produces high strength and good ductility. In addition, the strengthening effect of stacking faults was also demonstrated in brittle materials, such as gallium arsenide semiconductor nanowires [14] and silicon carbide ceramic nanorods [10]. That is, similar to TBs, the influence of stacking faults on the mechanical properties and deformation mechanism is closely related to the interaction between dislocations and stacking faults. However, there has been no systematic research aiming

Abbreviations: CSF, Complex stacking fault; FCC, Face-centered-cubic; Ni_3Al, Nickel aluminide; SC, Single crystal; SISF, Superlattice intrinsic stacking fault; TB, Twin boundary.

* Corresponding author.
E-mail address: wangjun@lnm.imech.ac.cn (J. Wang).

https://doi.org/10.1016/j.ijmecsci.2021.106953
Received 22 June 2021; Received in revised form 11 October 2021; Accepted 18 November 2021
Available online 26 November 2021

at the effect of stacking faults on strength and ductility of FCC materials.

Ni_3Al is an intermetallic ordered alloy with the $L1_2$ structure, where Al atoms occupy corners and Ni atoms take over face centers of an FCC cell. Due to its potential corrosion, oxidation and creep resistance, high strength and good thermal properties, Ni_3Al has been widely applied in aerospace industries such as turbine blades and vanes in aircraft engines [15–19]. Extensive experimental and theoretical efforts have been made to elucidate the structural and mechanical properties of single crystal Ni_3Al (SC-Ni_3Al) [20]. However, the low susceptibility to plastic deformation and the high tendency to brittle cracking strongly limit their industrial applications [21]. Through nanostructural design, some metallic materials can achieve strengthening and toughening [22–25]. For instance, Wang et al. [26] investigated plastic deformation and failure mechanisms of Ni_3Al nanowires with TBs (TB-Ni_3Al). Their results indicated that strength, ductility and fracture toughness of TB-Ni_3Al increase simultaneously with reducing the spacing between neighboring TBs.

The super-lattice structure of Ni_3Al increases the complexities of microstructures and consequently, the modes of deformation. Depending on the diversities of dislocation reactions, there are kinds of stable stacking faults in Ni_3Al, e.g., superlattice intrinsic stacking fault (SISF), antiphase boundary and complex stacking fault (CSF) [27,28]. For deformation in Ni_3Al, one stable dissociation of dislocations is that a <110> super-dislocation dissociates into two 1/2<110> super-partials bounding with an antiphase boundary on (111) and (010) planes, respectively. The other stable dissociation of the <110> super-dislocation also generates two 1/3<112> Shockley super-partial dislocations bounding with an SISF. The metastable dissociation of a <110> super-dislocation brings one 1/2<110> super-partial and two 1/6<112> Shockley partials bounding with a CSF. In addition, the structure of TBs can also be considered as 'thick' stable stacking faults. Studying these stacking faults is pivotal to a better understanding of strength and ductility of nanostructured Ni_3Al. Here, the size of stacking faults plays a major role in dislocation mobility, which drastically affects the mechanical properties of Ni_3Al. However, previous studies are mainly concentrated on the energy of stacking faults in nanostructured Ni_3Al by first-principles calculations [27,28]. In contrast, there are relatively few investigations in molecular dynamics simulations, which can establish an all-atom model to examine the mechanical properties of nanostructured Ni_3Al nanowires.

In this paper, stacking faults are introduced into Ni_3Al to investigate whether their configurations could strengthen and toughen Ni_3Al nanowire in comparison with nanoscale TBs. By using molecular dynamics simulations, a series of SC-Ni_3Al, CSF-Ni_3Al, SISF-Ni_3Al and TB-Ni_3Al nanowires under uniaxial tension have been modeled with various spacings between the planar defects. Numerical results are discussed in terms of their stress-strain curves, Young's modulus, yield strength, and the corresponding uniform elongation, i.e., strain at which necking occurs during a tensile process.

2. Numerical models and methodology

2.1. Nanostructured Ni_3Al models

Based on the stacking sequences of SC-, CSF-, SISF- and TB-Ni_3Al as illustrated in Fig. 1a–d, models can be established on the fact that Ni_3Al adopts a close-packed structure with an arrangement of three successive planes, denoting as A, B and C, along the [111] direction (see Fig. 1e). Here, SC-Ni_3Al is built up according to the $L1_2$ crystal structure with periodic repeat of the ABC stacking sequence. CSF-Ni_3Al and SISF-Ni_3Al models are formed by shearing C with $a/6[11\bar{2}]$ (111) and $a/3[11\bar{2}]$ (111), respectively [27], with a the lattice constant of Ni_3Al. An SISF--Ni_3Al with a spacing of 0.9 nm between parallel SISFs corresponds to a stacking sequence of ABC***AC*** as a periodically repeating unit, where bold and italic letters represent planar defects. Whereas a CSF-Ni_3Al with the same spacing between parallel CSFs consists of a stacking sequence of ABC***AC**** as a periodic unit. Here, the ***C**** layer adopts an alternative arrangement of atoms in contrast to that of C layer in an SISF-Ni_3Al [27]. The corresponding unit of a periodically stacking sequence of TB-Ni_3Al is ***C***BAC***B***CAB, with a spacing of 0.9 nm between parallel TBs. These planar defects of Ni_3Al were characterized through the experimental observation with a transmission electron microscopy [29,30], indicating

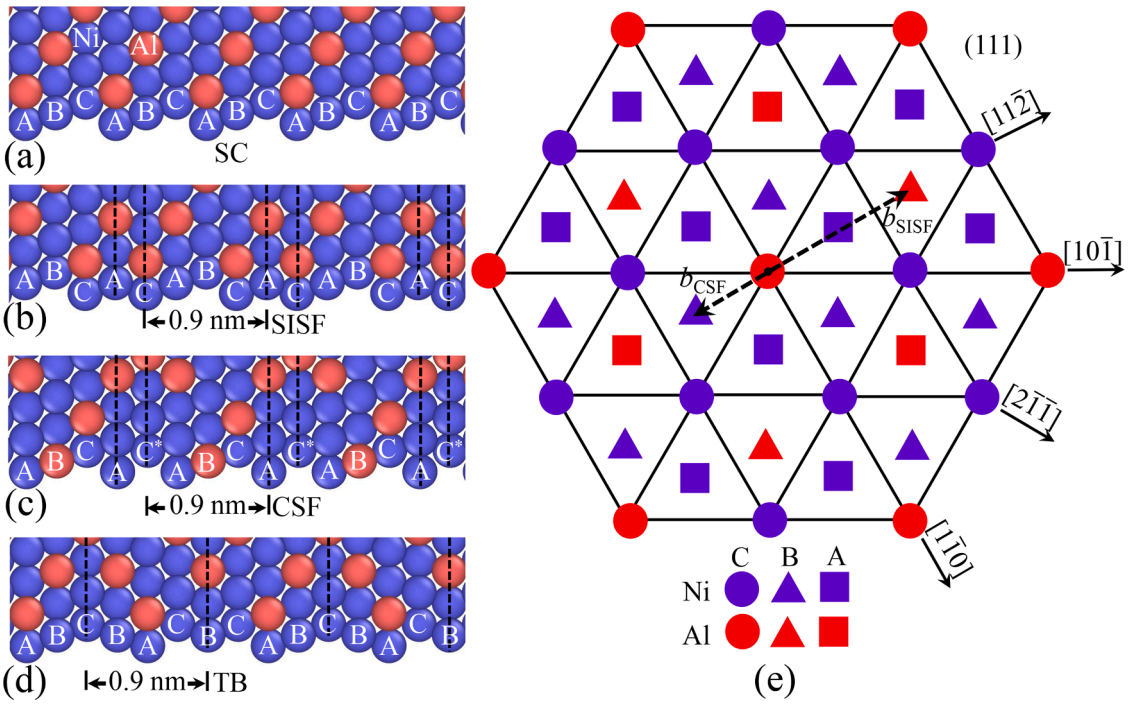

Fig. 1. The stacking sequence of nanostructured $L1_2$ Ni_3Al with (a) SC, (b) SISF, (c) CSF and (d) TB with a spacing of 0.9 nm between parallel planar defects. (e) The atomic arrangement of $L1_2$ structure in top view. A, B and C represent close-packed sites. Operation with the vectors b_{SISF} and b_{CSF} generates SISF and CSF, respectively.

that the intrinsic planar defects play an important role in the plastic deformation processes of Ni-based superalloys.

The typical models of nanostructured Ni_3Al are sketched in Fig. 2, including CSF, SISF and TB models with a spacing of 0.9 nm between planar defects. All these wires were created in a cylindrical lateral shape with an aspect ratio of length (L) to diameter ($D = 6$ nm) at least larger than 3.0. Spacing between planar defects varies from 0.9 nm (i.e., the smallest spacing to ensure a complete ABC stacking sequence of $L1_2$ structure along the [111] direction) to 10.7 nm. In order to show the changing tendency of yield strength, uniform elongation and Young's modulus versus spacing, five simulations were performed for each spacing. An SC nanowire was taken as a reference to investigate the strengthening and toughening effect of TBs, SISFs and CSFs. Each model contains up to ~80,000 atoms, depending on the length of a nanowire.

2.2. Molecular dynamics simulation

Atomistic simulations were performed by using the Largescale Atomic/Molecular Massively Parallel Simulator [31]. An embedded-atom method potential function for the Ni-Al system developed by Mishin [32] was taken to describe the atomic interaction in Ni_3Al. In this function, the total energy, E, of a system is depicted as

$$E = \sum_{\substack{ij \\ i \neq j}} V_{EAM}(r_{ij}) + \sum_i F(\overline{\rho}_i), \tag{1}$$

where $V_{EAM}(r_{ij})$, a pair potential, is a function of the distance r_{ij} between atoms i and j. Moreover, F is the embedding energy of atom i, and $\overline{\rho}_i$ is the electron density, which is written as

$$\overline{\rho}_i = \sum_{i \neq j} g_j(r_{ij}), \tag{2}$$

where $g_j(r_{ij})$ is the electron density of atom j.

Such a potential was built up by fitting to data of both experiments and first-principles. It can depict an accurate lattice, the mechanical properties, and especially energetics of point defects and planar faults. The latter is essential to study planar faults dominated deformation mechanisms of Ni_3Al [33].

Periodic boundary conditions were introduced in the Z-[111] crystalline directions. Simulations were performed by integrating Newton's equations of motion for all atoms with a time step of 1 fs. At the beginning of simulation, Ni_3Al nanowires were energetically minimized by relaxing a sample for 100 ps at 300 K. To obtain the mechanical properties, a uniaxial tensile load along the [111] direction (perpendicular to planes of CSFs, SISFs and TBs) was applied with a constant strain rate of 5×10^8 s^{-1}. Stress in a stress-strain relationship was calculated by the Virial scheme, which was usually used in atomistic simulations [34–37]. Young's modulus was fitted from the ~2% elastic regime of a stress-strain curve. During uniaxial loading, transverse directions were permitted to relax and kept a stress-free condition. Deformation and defects of Ni_3Al nanowires were recognized by common neighbor and dislocation analysis and then, visualized by the software OVITO [38].

3. Simulation results

3.1. Tensile stress-strain relationships

As shown in Fig. 3a, all stress-strain curves of Ni_3Al nanowires linearly rise in stress with the increase of strain until their yield strength. After that, stress encounters a sudden drop and then undergoes fluctuation with further increasing strain. However, these four curves do not synchronize. Specifically, the SISF-Ni_3Al nanowire yields the biggest yield strength of 17.2 GPa, whilst the CSF-Ni_3Al nanowire generates the smallest yield strength of 15.2 GPa. Between them, TB-Ni_3Al has bigger yield strength (16.4 GPa) than that of CSF-Ni_3Al, but it is still less than that (16.9 GPa) of SC-Ni_3Al. The uniform elongation of four nanowires keeps step with their corresponding yield strength, with values of 7.98%, 7.53%, 7.18% and 6.88% for SISF-, SC-, TB- and CSF-Ni_3Al, respectively.

Real-time detection on dislocation activities indicates that the stress-strain curves closely relate to their densities of dislocation lines (see Fig. 3b). Taking the CSF-Ni_3Al nanowire as an example, the first dislocation event (i.e., dislocation nucleation) is captured as yield strength is arrived. Then, the density of dislocation lines rapidly increases to its maximum value of 1.5×10^{-3} $Å^{-2}$ at the strain of 6.63%. This period echoes exactly to a sudden drop in stress from its peak value to 7.2 GPa. After that, the density of dislocation lines gradually reduces, corresponding to fluctuation of stress with the increase of strain. The highest density (2.7×10^{-3} $Å^{-2}$) of dislocation lines appears in the SISF-Ni_3Al nanowire at a strain of 7.63%. The SC-Ni_3Al nanowire, however, produces the lowest density of dislocation lines (1.4×10^{-3} $Å^{-2}$) as strain reaches 7.48%. The TB-Ni_3Al nanowire is the second one to attain its maximum value of density of dislocation lines (2.3×10^{-3} $Å^{-2}$) with a strain at 7.28%.

3.2. Deformation mechanisms of SC-Ni_3Al and TB-Ni_3Al

As seen in Fig. 4, as strain is less than 6.98%, there are no dislocations in the SC- Ni_3Al nanowire, declaring elastic deformation of it (Fig. 4a). Then, with strain increasing, a 1/6<112> Shockley dislocation nucleates on surface of the nanowire and propagates inward, forming a layer of tilted stacking faults behind it (Fig. 4b). As more 1/6<112> Shockley dislocations continuously nucleate and spread inside the nanowire, they meet to form a 1/6<110> stair-rod dislocation at their junction area (Fig. 4c). Finally, as illustrated in Fig. 4d, when strain reaches 14.98%, the dislocation density falls to its minimum due to annihilation of dislocations on surface of the nanowire. This can be postponed by introducing planar defects such as SISFs and TBs. Residual dislocations in the deformed nanowire are mainly 1/6<112> Shockley type, accompanied by multiple tilted stacking faults.

In contrast to that in the SC- Ni_3Al nanowire, dislocations first nucleate on surface of a TB-Ni_3Al nanowire adjacent to a TB and then spread inward at a strain of 6.88% (Fig. 5a). As dislocations move to a TB, they are impeded and react with TB. Reaction brings 1/6<110> stair-rod and 1/3<111> Frank dislocations, accounting for the density of dislocation lines of 8.00% and 8.60%, respectively. Reaction also sets off migration and detwinning of TB as shown in Fig. 5b. With strain increasing to 7.23%, TB migrates downward and the pinning effect is observed above it. Dislocations participating pinning are mainly 1/6<112> (69.70%) and a small amount of 1/6<110> stair-rod, 1/3<100> Hirth, and 1/2<110> perfect (see Fig. 5c). Consequently, necking happens at the site of TB. Further increase in strain induces serious necking and more pinning events as illustrated in Fig. 5d. It is worth noting that, however, there is no dislocation passing through TBs during stretching of a TB-Ni_3Al nanowire.

3.3. Deformation mechanisms of CSF-Ni_3Al and SISF-Ni_3Al

As shown in Fig. 6, at a strain of 6.33%, a 1/6<112> Shockley dislocation nucleates on surface of nanowire near a CSF, and then, it spreads obliquely inward with a tilted stacking fault left behind it. As it meets the CSF, such a dislocation stimulates a new 1/6<112> Shockley dislocation on CSF. Finally, with the original dislocation cutting through CSF, the stimulated one spreads transversely along CSF. Transverse propagation of the stimulated 1/6<112> dislocation causes fading of CSF (see Fig. 6a). As strain reaches 6.48%, the transversely moving dislocation has gone out of surface of the nanowire, resulting in complete fading of CSF on which it once moves. Meanwhile, the original 1/6<112> dislocation meets another CSF. It induces a new 1/6<112> dislocation and crosses over CSF to continue its movement. Here, the second generated dislocation propagates obliquely without causing

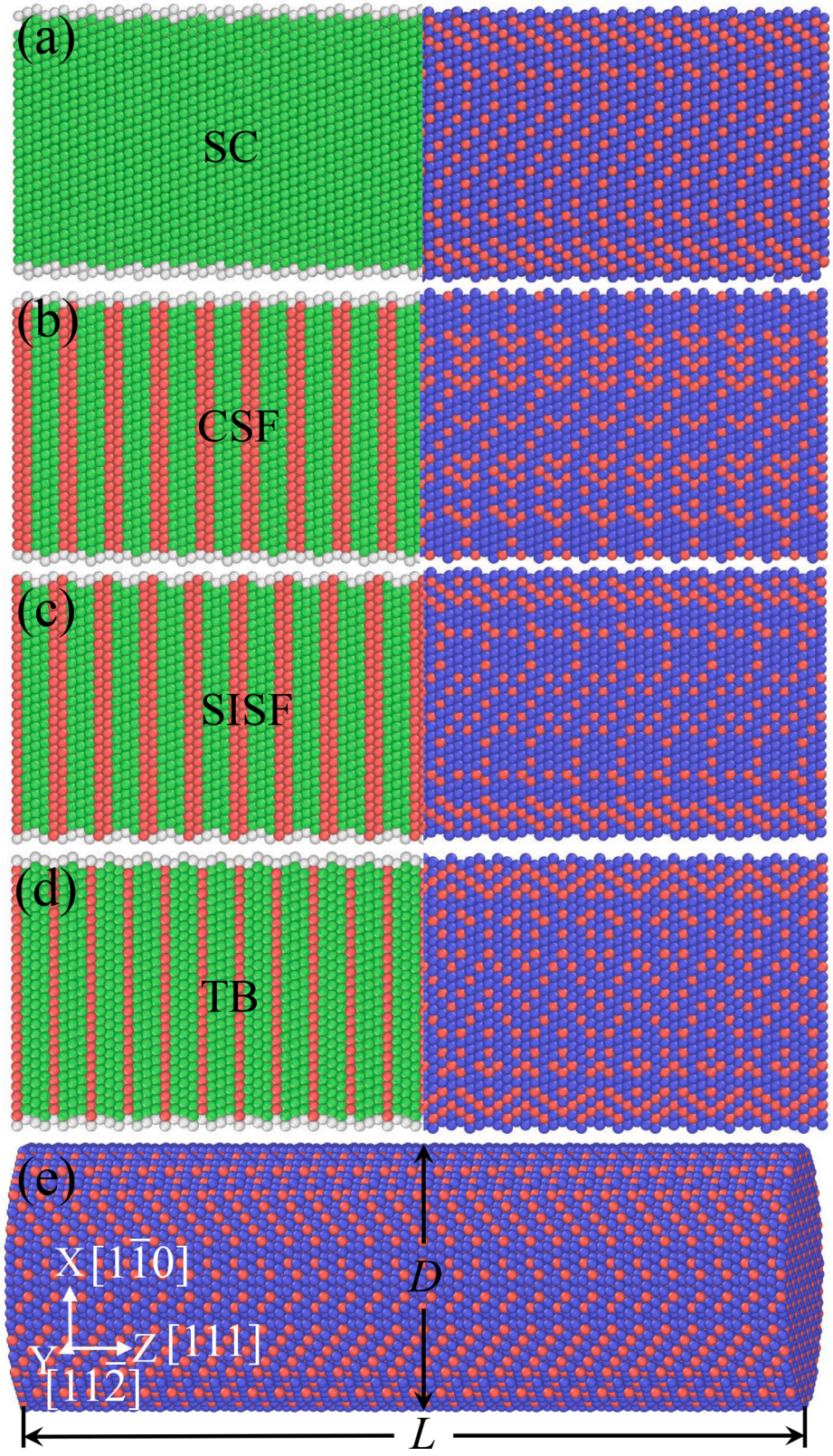

Fig. 2. Tensile models of nanostructured Ni_3Al nanowires, including cross-section diagrams of (a) SC-, (b) CSF-, (c) SISF- and (d) TB-Ni_3Al nanowires. Spacing between parallel planar defects is 0.9 nm. To show planar defects, a half nanowire is colored by common neighbor analysis with green and red representing the FCC structure and planar defects. (e) The cylindrical shape of an SC-Ni_3Al nanowire with length $L = 18$ nm and diameter $D = 6$ nm.

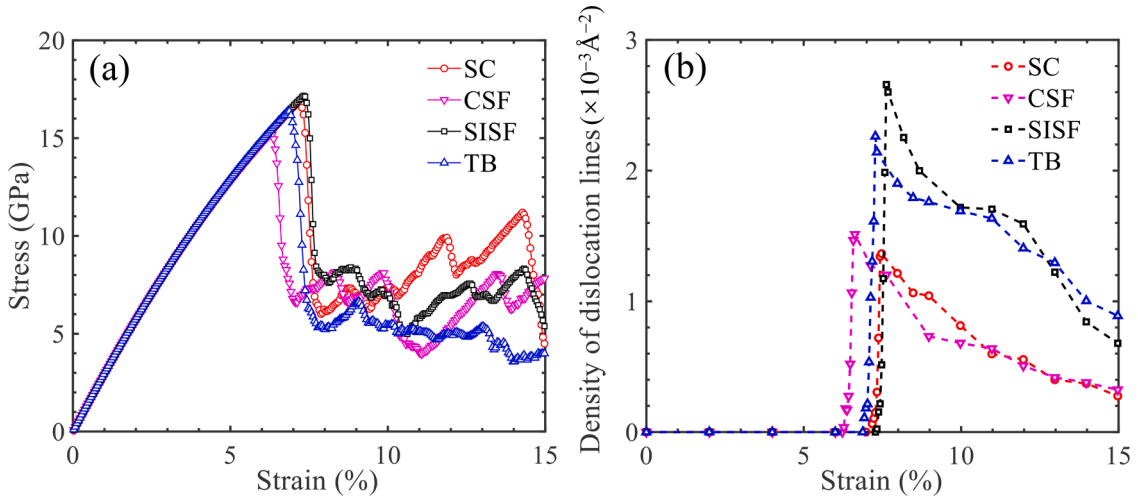

Fig. 3. (a) Typical tensile stress-strain relationships and (b) their corresponding densities of dislocation lines in nanostructured Ni_3Al nanowires with a spacing of 4.5 nm between parallel planar defects.

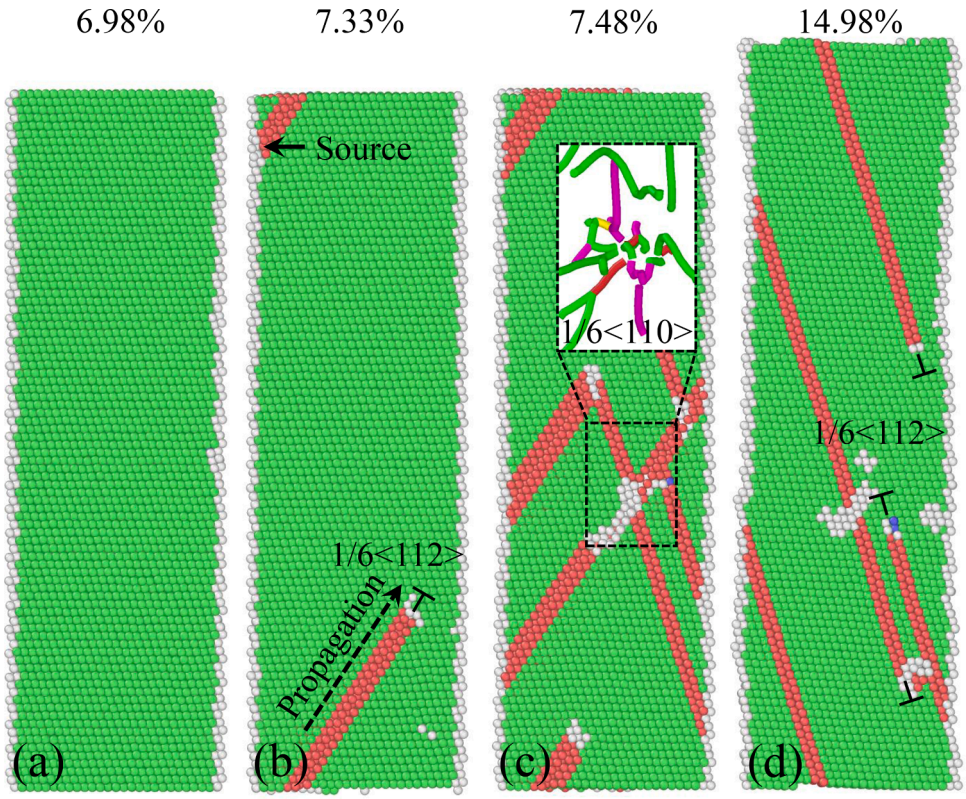

Fig. 4. Atomic configurations of an SC-Ni_3Al nanowire with a diameter of 6.0 nm under uniaxial stretching at various tensile strains of (a) 6.98%, (b) 7.33%, (c) 7.48% and (d) 14.98%, where atoms are colored by common neighbor analysis. Inset in (c) shows the structure of local dislocations visualized by dislocation analysis with green, purple, yellow and red lines indicating 1/6<112> Shockley, 1/6<110> stair-rod, 1/3<100> Hirth, and other kind of dislocations, respectively.

fading of CSF (see Fig. 6b). Moreover, more 1/6<112> dislocations nucleate on surface of the nanowire and moves inward. Further increase in strain induces more dislocation activities as shown in Fig. 6c–e. Detection on dislocation activities also captures other types of dislocations such as 1/6<110> stair-rod, 1/3<100> Hirth, and 1/2<110> perfect (see local enlarged drawings in Fig. 6d and e). However, these dislocations do not contribute to fading of CSFs.

Adjacent to intersections between SISFs and the surface of a nanowire, 1/6<112> Shockley dislocations nucleate and propagate inward as strain passes by 7.38% (see Fig. 7a). With strain increasing, 1/6<112> dislocations propagate to encounter SISFs. As they overcome obstacles, new 1/6<112> dislocations are stimulated at SISFs (Fig. 7b and c). Interaction between an original 1/6<112> and a new stimulated one near SISFs produces a 1/6<110> stair-rod on SISFs (see Fig. 7d and e). The 1/6<110> stair-rod does not propagate and keeps SISFs without fading with the increase of strain. Near SISFs, the 1/6<110> stair-rod pins other types of dislocations such as 1/2<110> perfect, 1/3<100> Hirth, and 1/6<112> Shockley (amplified regions in Fig. 7d and e). These pinned dislocations consist of 1.20%, 7.80% and 66.70%, respectively, in the density of dislocation lines at a strain of 14.98%.

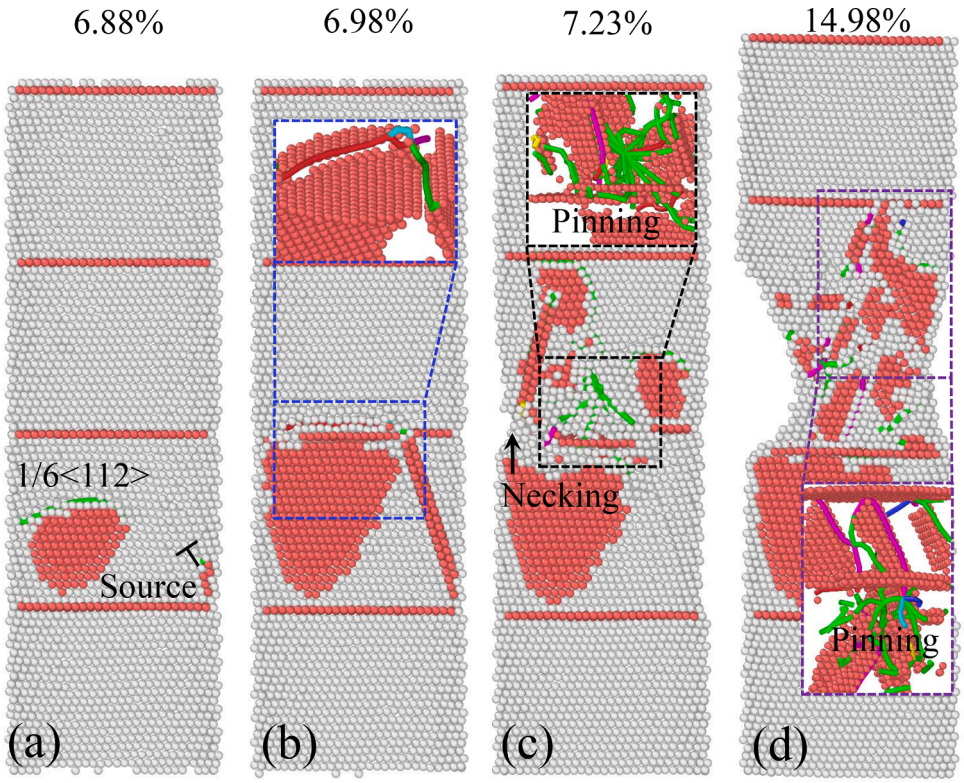

Fig. 5. Atomic configurations of a TB-Ni_3Al nanowire with a spacing of 4.5 nm between parallel TBs under uniaxial tension at various strains of (a) 8.38%, (b) 8.53%, (c) 9.98% and (d) 14.98%, where atoms are colored by the dislocation analysis and FCC structures are removed for clarity. Insets in (b–d) show the structures of local dislocations.

3.4. Effects of the spacing between planar defects

The mechanical properties of nanostructured Ni_3Al nanowires significantly depend on spacing between planar defects, as summarized in Fig. 8. Strengthening is achieved in SISF- and TB-nanowires. The yield strength of SISF-nanowires increases by 11.3% from 16.8 to 18.7 GPa with spacing between planar defects reducing from 10.7 to 0.9 nm. TB-nanowires brings a 16.0% growth of yield strength from 16.2 to 18.8 GPa at the same spacing range. Both SISF- and TB-nanowires possess an ability to exceed yield strength of an SC-nanowire as spacing between parallel planar defects is reduced less than 4.5 and 2.1 nm for SISF and TB, respectively (see Fig. 8a). The yield strength σ_Y of SISF- and TB-Ni_3Al nanowires follows the Hall-Petch relationship, that is

$$\sigma_Y = \sigma_0 + \frac{k}{d^n}, \tag{3}$$

where σ_0 and k are the material and structural dependent parameters, d is spacing between parallel planar defects, and n is an exponent. By fitting simulation results of nanowires with a diameter of 6 nm to Eq. (3), the constants σ_0 and k can be determined as 16.4 GPa and 1.8 nm^{-1} for SISF-Ni_3Al nanowires and 14.6 GPa and 3.5 $nm^{-1/2}$ for TB-Ni_3Al nanowires, respectively. Variation of the diameter just produces alternative values of σ_0 and k in Eq. (3) since the sample size has been implied within them. Most importantly, the values of n are 1 and 1/2 for SISF-Ni_3Al and TB-Ni_3Al nanowires, respectively (see Fig. 8a). Here it is of interest to note that there is no inverse Hall-Petch effect even as spacing between parallel planar defects is cut down to its lower end of 0.9 nm (see Appendix A for the structural evolution of nanowires under uniaxial tension). Fig. 8b further indicates that the uniform elongation of SISF- and TB-nanowires goes beyond that of an SC-nanowire as spacing between planar defects is less than 4.5 and 2.1 nm, respectively. On the contrary, there is no strengthening in CSF-nanowires. Their yield strengths are always lower than that of an SC-nanowire. Moreover, neither the uniform elongation nor Young's modulus of them can compete with that of an SC-nanowire (see Fig. 8b and c).

4. Discussion

To validate the values of yield strength generated by various microstructures, we have checked available theoretical and experimental data. Specifically, the yield strengths (16.2–18.8 GPa) of TB-Ni_3Al obtained are well consistent with that (14.8–16.8 GPa) of Ni_3Al twinning nanopillars from molecular dynamics simulations [26]. Obviously, these values are smaller than the ideal tensile strength (~25.0 GPa) of Ni_3Al along the [111] orientation according to the first-principle calculation [39]. Here it is worth noting that the first principle can only estimate the upper bound of yield strength without taking temperature, sample size or strain rate into account. We also note that the yield strength (16.9 GPa) of the [111] oriented SC-Ni_3Al nanowire is larger than that (10.2 GPa) of Ni_3Al nanocubes with [100] orientation determined from experiments [20]. This is because that the sample size, crystalline orientation and strain rate have significant effects on the yield strength of Ni_3Al. Specifically, Li et al. [40] indicated that the yield strength of dislocation-free Ni_3Al nanocubes increases from ~2.1 to ~4.5 GPa as the sample size reduces from ~630 to ~180 nm, with up to 1–2 orders of magnitude higher than that of bulk Ni_3Al [41]. This agrees with the theoretical modeling on the size-dependent yield strength of Ni_3Al micro-pillars [42,43]. In addition, Zhu et al. [44] elucidated that the yield strength at a strain rate of 10^8 s^{-1} (corresponding to the scenario of molecular dynamics) is 2–3 times higher than that below a strain rate of 10^{-2} s^{-1} (i.e., the experimental results at quasi-static loading conditions).

The simulation results can be further validated by the size and strain rate effects on yield strength and uniform elongation of SC-Ni_3Al nanowires. Fig. 9 shows that, as the diameter of nanowires increases from 3 to 12 nm, the yield strength decreases from 19.0 to 16.1 GPa and

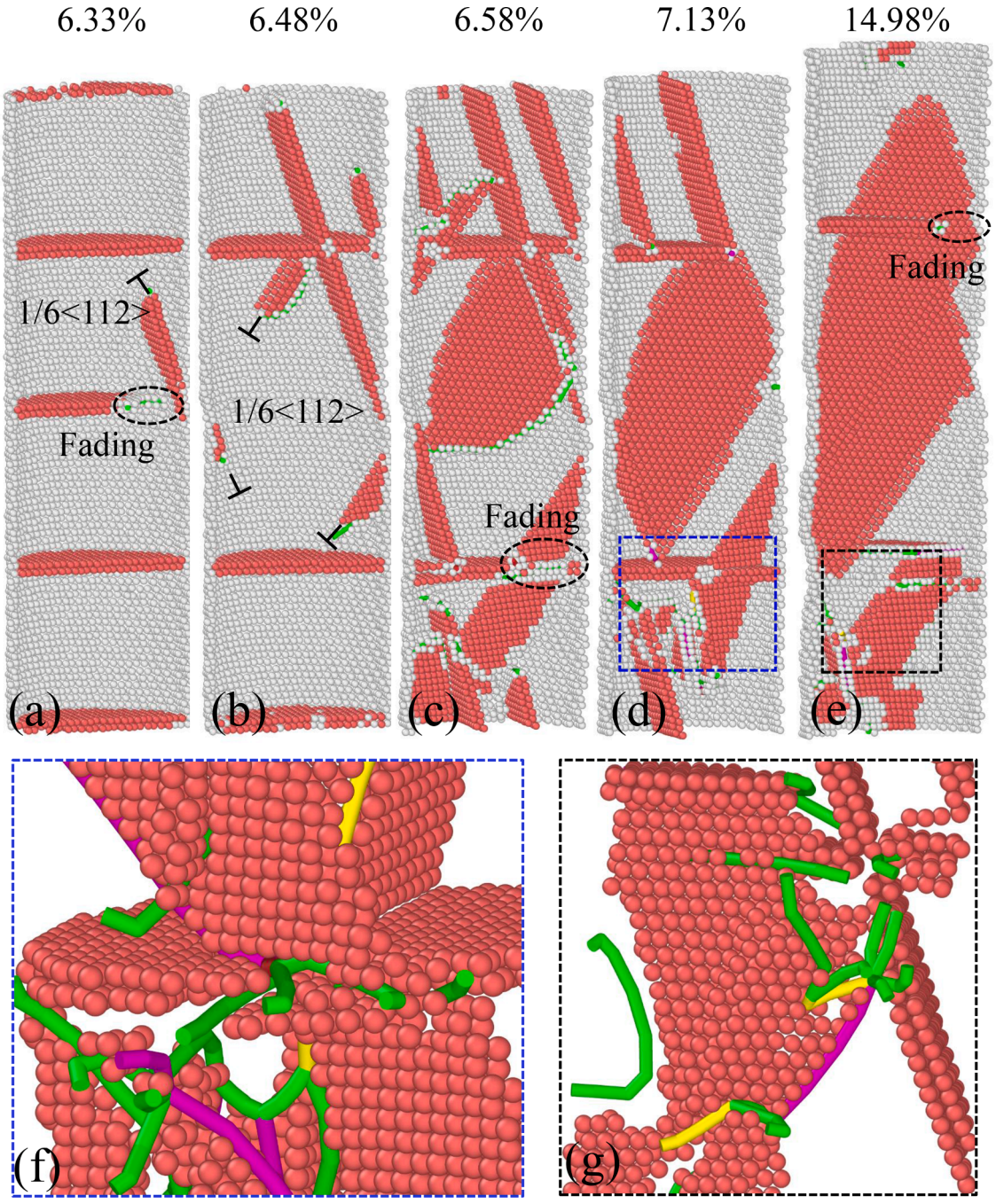

Fig. 6. Evolution of microstructures analyzed by the dislocation analysis with strain increasing in a CSF-Ni_3Al nanowire with a spacing of 4.5 nm between parallel CSFs. (a) a 1/6<112> Shockley dislocation nucleates on surface of a nanowire and causes fading of CSF (marked by a dashed ellipse) to which it spreads. (b) Motion, nucleation and interaction of 1/6<112> Shockley with another CSF. (c), (d) and (e) More dislocation activities at various strains. (f) and (g) Local enlarged structures in areas marked by dash boxes in (d) and (e). Structures of dislocations at local regions such as 1/6<112> Shockley, 1/6<110> stair-rod and 1/3<100> Hirth are expressed with green, purple and yellow lines, respectively, and FCC structures are removed for clarity.

the uniform elongation falls from 8.3 to 7.1%. In addition, as the strain rate increases from 5×10^6 to 5×10^{10} s^{-1}, the yield strength rises from 15.5 to 21.1 GPa and the uniform elongation grows from 6.7 to 11.1% (see Fig. 10). Although there is still a huge difference in comparison with the size and strain rate in experiments, the changing trends are well consistent with experimental observation and theoretical description [41,44]. Hence, taking account of the size and strain rate effects, it is reasonable to conclude that the [111] oriented SC-Ni_3Al nanowire with a lateral dimension of 6 nm has a yield strength of 16.9 GPa at a strain rate of 5×10^8 s^{-1}.

Ductility is usually measured by the uniform elongation or the elongation to failure [45]. In this work, uniform elongation is employed to characterize ductility because it is not affected by the geometry and size of a sample. As shown in Fig. 8, the uniform elongation and yield strength of nanostructured Ni_3Al nanowires significantly depend on the type of planar defects. Their deformation mechanisms are attributed to the diversity of interactions between dislocations and planar defects. These interactions produce both profitable and disadvantageous aspects. Profitable factors include impediment of planar defects to propagation of dislocations and pinning of dislocations at a local region. Disadvantages consist of fading of planar defects, detwinning and migration of TBs. In all kinds of nanowires, the first dislocation activity is nucleation

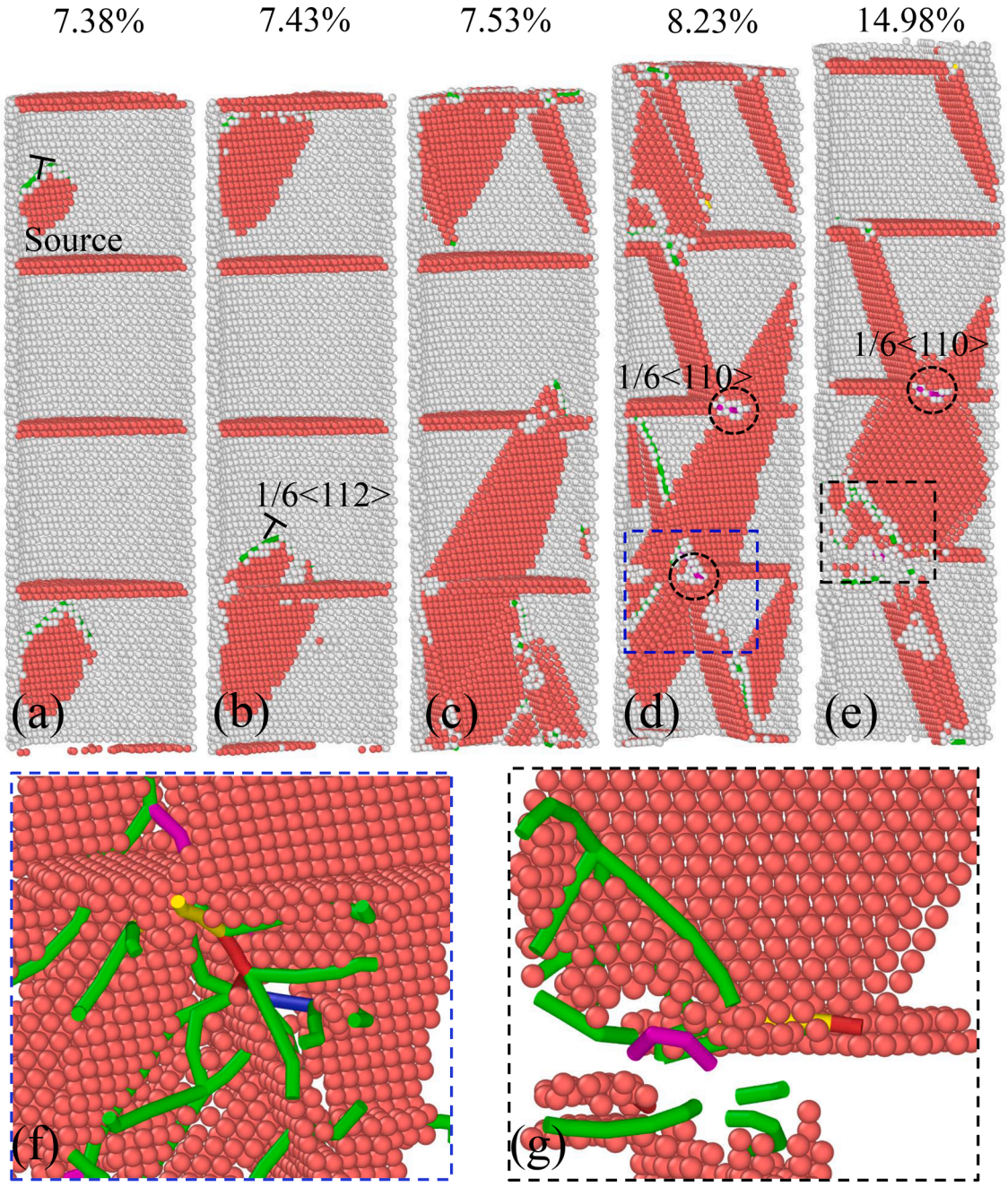

Fig. 7. Dislocation activities in an SISF-Ni_3Al nanowire under uniaxial tension. Spacing between parallel SISFs is 4.5 nm. (a) 1/6<112> Shockley dislocations initiate on surface of a nanowire and (b) propagate inward. (c) Dislocations cross over SISFs. (d) and (e) Interaction between 1/6<112> Shockley dislocations and SISFs brings 1/6<110> stair-rod dislocations (indicated by dashed circles) which pin dislocations near SISFs. (f) and (g) Local enlarged structures in areas marked by dash boxes in (d) and (e). Microstructural evolution is analyzed by the dislocation analysis, with surface and planar defects being colored in white and red. 1/6<112> Shockley, 1/2<110> perfect, 1/6<110> stair-rod and 1/3<100> Hirth dislocations are shown with green, blue, purple and yellow lines.

of the 1/6<112> Shockley dislocation. It accounts for more than 60% density of dislocation lines at an arbitrary strain after its appearance. They can cut through CSFs and SISFs but be stopped by TBs. Interaction between a 1/6<112> and a CSF induces fading of CSF. Thus, lack of obstacle to propagation of dislocations weakens the yield strength and uniform elongation of CSF-Ni_3Al nanowires. On the contrary, in SISF--Ni_3Al nanowires, the stability of a 1/6<110> stair-rod helps to pin dislocations near an SISF, bringing strengthening and toughening. Pinning effect and obstacle of TBs to motion of dislocations are reasons for improvement of yield strength of TB-Ni_3Al nanowires. However, detwinning and migration reduce yield strength, declaring the poor performance of TBs to strengthen in comparison with that of SISFs with the same spacing between planar defects (see Fig. 8a). Strengthening of both SISFs and TBs can be described by the Hall-Petch relationship, with the exponent of 1 and 1/2, which echo experimental results measured from Mg alloy containing stacking faults [11,12] and nanotwinned copper [8,9,46], respectively.

In addition, it is worth noting that the yield strength sharply decreases with the increase of spacing between TBs (or SISFs) from 0.9 to 3.3 nm. However, there is not a noticeable decrease with further increase of spacing (see Fig. 8a). The similar trends were observed in experiments of Mg alloy with stacking faults and copper with TBs [12,46]. The reason for this is that, the smaller the spacing between planar defects, the more obvious the hindering effect of planar defects to

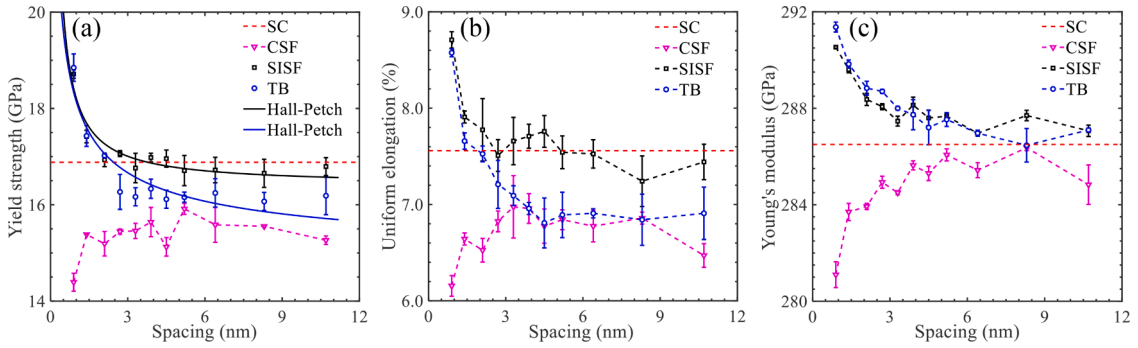

Fig. 8. The mechanical properties of nanostructured Ni_3Al nanowires depend on spacing between planar defects. (a) The yield strength with solid lines fitted by Eq. (3), (b) uniform elongation, and (c) Young's modulus vary with spacing between planar defects.

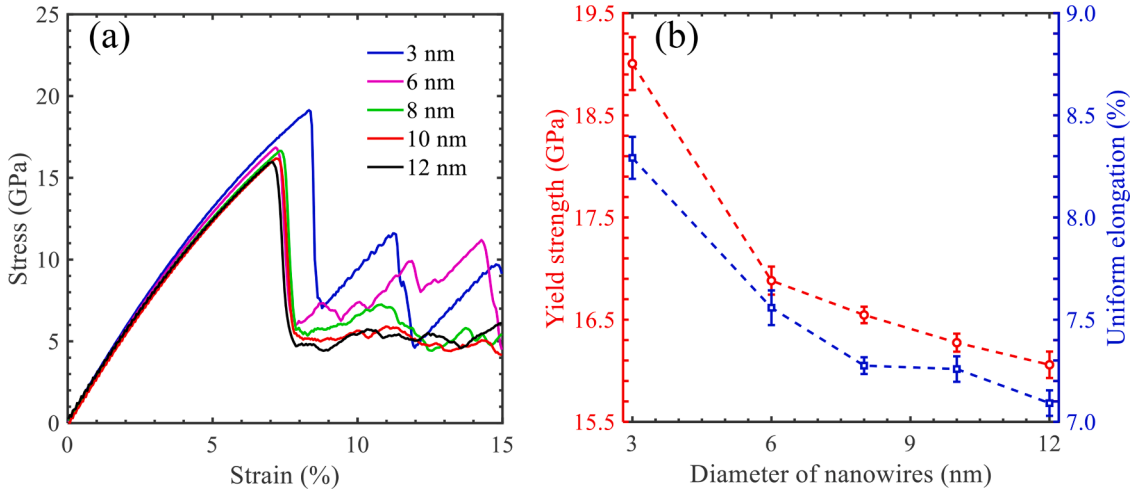

Fig. 9. The sample size effect on the mechanical properties of SC-Ni_3Al nanowires with a strain rate of 5×10^8 s^{-1}. (a) Stress-strain curves and (b) the yield strength and uniform elongation.

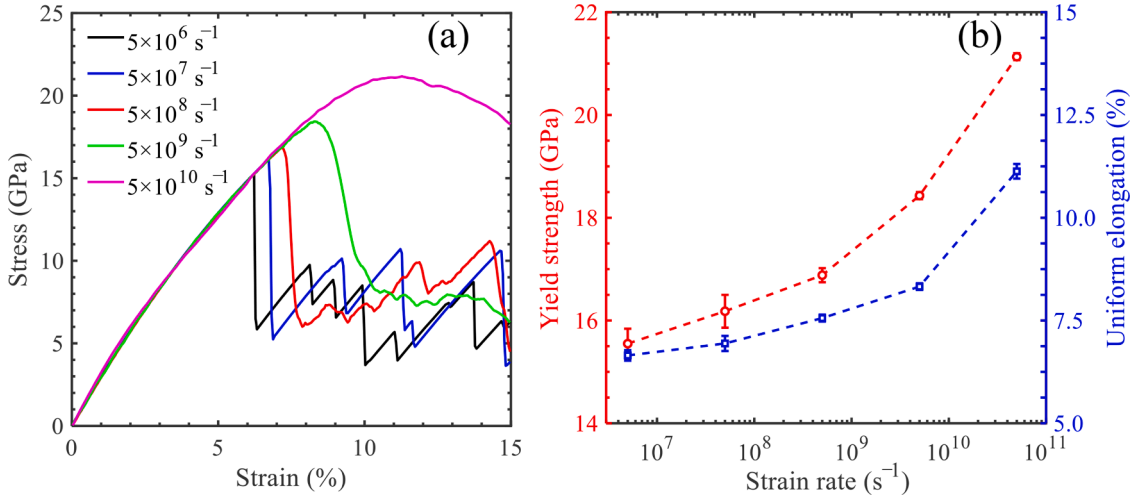

Fig. 10. The strain rate effect on the mechanical properties of SC-Ni_3Al nanowires with a diameter of 6 nm. (a) Stress-strain curves and (b) the yield strength and uniform elongation.

dislocation activities is. When the spacing between planar defects is beyond 3.3 nm, the contribution of planar defects to yield strength is inappreciable. This is in agreement with the Hall-Petch relationship. That is, since the variation of yield strength is proportional to $d^{-(n+1)}$, the sharply reduced yield strength tends to be stable with the increase of spacing.

The microstructural dependent Young's modulus of Ni_3Al nanowires is attributed to the energetic stability of CSFs, SISFs and TBs. Based on analysis of first principles, the energy of a CSF is nearly two times over that of an SISF, while an SISF and a TB possess roughly the same energy [26,27,33,47–49]. Since Young's modulus represents the ability of a material to resist elastic deformation, the energetic instability cuts down

such an ability. This leads to a lower Young's modulus of CSF-Ni_3Al nanowires in contrast to that of SISF- and TB-Ni_3Al nanowires.

5. Conclusion

In summary, a series of molecular dynamics simulations of nanostructured Ni_3Al nanowires have been performed under uniaxial tension. The mechanical properties and deformation mechanisms of nanostructured Ni_3Al nanowires have been clarified. It is shown that, the yield strength and uniform elongation of nanostructured Ni_3Al nanowires significantly depend on the type of planar defects. The different deformation mechanisms are due to the diversity of interactions between dislocations and planar defects. The main conclusions can be summarized as follows:

(1) In contrast to CSFs, strengthening and toughening can be achieved with SISFs and TBs. the favorable factors are attributed to impediment of planar defects to propagation of dislocations and pinning effect resulting from interaction between dislocations and planar defects. Disadvantageous aspects include fading of planar defects, detwinning and migration of TBs.
(2) Among these nanowires, SISF-Ni_3Al nanowires gain the best strengthening and toughening, and CSF-Ni_3Al nanowires have the worst mechanical properties. Strengthening by SISFs and TBs can be described by the Hall-Petch relationship with an exponent of 1 and 1/2, respectively.
(3) The Young's modulus of nanostructured Ni_3Al nanowires depends on their energetic stability of nanostructures. In contrast to SISF- and TB-Ni_3Al nanowires, CSF-Ni_3Al nanowires have a lower Young's modulus.

It is expected that these findings could provide new insights into a deep understanding on deformation mechanisms of nanostructured Ni_3Al and benefit its optimal design and wide application in the aerospace industry.

CRediT authorship contribution statement

Zhiwei Zhang: Conceptualization, Investigation, Methodology, Data curation, Writing – original draft. **Qiang Fu:** Formal analysis. **Jun Wang:** Conceptualization, Supervision, Writing – review & editing, Funding acquisition. **Rong Yang:** Writing – review & editing. **Pan Xiao:** Funding acquisition. **Fujiu Ke:** Conceptualization. **Chunsheng Lu:** Writing – review & editing.

Declaration of Competing Interest

The authors declare that they have no known competing financial interests or personal relationships that could have appeared to influence the work reported in this paper.

Acknowledgments

This work has been supported by the National Natural Science Foundation of China (Grant Nos. 11772332 and 11790292), the Strategic Priority Research Program of the Chinese Academy of Sciences (Project No. XDB22040501), and the Opening Fund of State Key Laboratory of Nonlinear Mechanics. The simulations were performed on resources provided by the ScGrid of Supercomputing Center, Computer Network Information Center of the Chinese Academy of Sciences, the LNMGrid of the State Key Laboratory of Nonlinear Mechanics, and the Pawsey Supercomputing Center with funding from the Australian Government and the Government of Western Australia.

Supplementary materials

Supplementary material associated with this article can be found, in the online version, at doi:10.1016/j.ijmecsci.2021.106953.

References

[1] Ovid'Ko IA, Valiev RZ, Zhu YT. Review on superior strength and enhanced ductility of metallic nanomaterials. Prog Mater Sci 2018;94:462–540.
[2] Zhu YT, Liao XZ, Wu XL. Deformation twinning in nanocrystalline materials. Prog Mater Sci 2012;57:1–62.
[3] Wu XL, Jiang P, Chen L, Yuan FP, Zhu YT. Extraordinary strain hardening by gradient structure. Proc Nat Acad Sci USA 2014;111:7197–201.
[4] Wu XL, Yang MX, Yuan FP, Wu GL, Wei YJ, Huang XX, Zhu YT. Heterogeneous lamella structure unites ultrafine-grain strength with coarse-grain ductility. Proc Nat Acad Sci USA 2015;112:14501–5.
[5] Ma XL, Huang CX, Xu WZ, Zhou H, Wu XL, Zhu YT. Strain hardening and ductility in a coarse-grain/nanostructure laminate material. Scr Mater 2015;103:57–60.
[6] Zhang ZW, Fu Q, Wang J, Yang R, Xiao P, Ke FJ, Lu CS. Interaction between the edge dislocation dipole pair and interfacial misfit dislocation network in Ni-based single crystal superalloys. Int J Solids Struct 2021;228:111128.
[7] Zhu YT, Narayan J, Hirth JP, Mahajan S, Wu XL, Liao XZ. Formation of single and multiple deformation twins in nanocrystalline fcc metals. Acta Mater 2009;57:3763–70.
[8] Lu L, Chen X, Huang X, Lu K. Revealing the maximum strength in nanotwinned copper. Science 2009;323:607–10.
[9] Li XY, Wei YJ, Lu L, Lu K, Gao HJ. Dislocation nucleation governed softening and maximum strength in nano-twinned metals. Nature 2010;464:877–80.
[10] Wang J, Shen YG, Song F, Ke FJ, Bai YL, Lu CS. Materials can be strengthened by nanoscale stacking faults. Europhys Lett 2015;110:36002.
[11] Jian WW, Cheng GM, Xu WZ, Koch CC, Wang QD, Zhu YT, Mathaudhu SN. Physics and model of strengthening by parallel stacking faults. Appl Phys Lett 2013;103:133108.
[12] Jian WW, Cheng GM, Xu WZ, Yuan H, Tsai MH, Wang QD, Koch CC, Zhu YT, Mathaudhu SN. Ultrastrong Mg alloy via nano-spaced stacking faults. Mater Res Lett 2013;1:61–6.
[13] Peng QM, Sun Y, Ge BC, Fu H, Zu Q, Tang XZ, Huang JY. Interactive contraction nanotwins-stacking faults strengthening mechanism of Mg alloys. Acta Mater 2019;169:36–44.
[14] Chen B, Wang J, Gao Q, Chen YJ, Liao XZ, Lu CS, Tan HH, Mai YW, Zou J, Rinfer SP, Gao HJ, Jagadish C. Strengthening brittle semiconductor nanowires through stacking faults: insights from *in situ* mechanical testing. Nano Lett 2013;13:4369–73.
[15] Seymour R, Hemeryck A, Nomura KI, Wang WQ, Kalia RK, Nakano A, Vashishta P. Nanoindentation of NiAl and Ni_3Al crystals on (100), (110), and (111) surfaces: a molecular dynamics study. Appl Phys Lett 2014;104:141904.
[16] Zhang ZW, Fu Q, Wang J, Xiao P, Ke FJ, Lu CS. Hardening Ni_3Al via complex stacking faults and twinning boundary. Comput Mater Sci 2021;188:110201.
[17] Zhang ZW, Fu Q, Wang J, Yang R, Xiao P, Ke FJ, Lu CS. Interactions between butterfly-like prismatic dislocation loop pairs and planar defects in Ni_3Al. Phys Chem Chem Phys 2021;23:10377–83.
[18] Zhang ZW, Fu Q, Wang J, Yang R, Xiao P, Ke FJ, Lu CS. Atomistic modeling for the extremely low and high temperature-dependent yield strength in a Ni-based single crystal superalloy. Mater Today Commun 2021;27:102451.
[19] Khoei AR, Eshlaghi GT, Shahoveisi S. Atomistic simulation of creep deformation mechanisms in nickel-based single crystal superalloys. Mater Sci Eng A 2021;809:140977.
[20] Maaß R, Meza L, Gan B, Tin S, Greer JR. Ultrahigh strength of dislocation-free Ni_3Al nanocubes. Small 2012;8:1869–75.
[21] Jozwik P, Polkowski W, Bojar Z. Applications of Ni_3Al based intermetallic alloys-current stage and potential perceptivities. Materials (Basel) 2015;8:2537–68.
[22] Li XW, Shi T, Li B, Chen XC, Zhang CW, Guo ZG, Zhang QX. Subtractive manufacturing of stable hierarchical micro-nano structures on AA5052 sheet with enhanced water repellence and durable corrosion resistance. Mater Des 2019;183:108152.
[23] Yang T, Zhao YL, Li WP, Yu CY, Luan JH, Lin DY, Fan L, Jiao ZB, Liu WH, Liu XK, Kai JJ, Huang JC, Liu CT. Ultrahigh-strength and ductile superlattice alloys with nanoscale disordered interfaces. Science 2020;369:427–32.
[24] Sun LG, Wu G, Wang Q, Lu J. Nanostructural metallic materials: structures and mechanical properties. Mater Today 2020;38:114–35.
[25] Li XW, Liang JS, Shi T, Yang DN, Chen XC, Zhang CW, Liu ZH, Liu DZ, Zhang QX. Tribological behaviors of vacuum hot-pressed ceramic composites with enhanced cyclic oxidation and corrosion resistance. Ceram Int 2020;46:12911–20.
[26] Wang YJ, Tsuchiya K, Dai LH. Size-dependent plastic deformation and failure mechanisms of nanotwinned Ni_3Al: insights from an atomistic cracking model. Mater Sci Eng A 2016;649:449–60.
[27] Wen YF, Sun J, Huang J. First-principles study of stacking fault energies in Ni_3Al intermetallic alloys. Trans Nonferr Metal Soc 2012;22:661–4.
[28] Yu XX, Wang CY. The effects of alloying elements on generalized stacking fault energies, strength and ductility of γ'-Ni_3Al. Mater Sci Eng A 2012;539:38–41.
[29] Zhao YL, Yang T, Li YR, Fan L, Han B, Jiao ZB, Chen D, Liu CT, Kai JJ. Superior high-temperature properties and deformation-induced planar faults in a novel $L1_2$-strengthened high-entropy alloy. Acta Mater 2020;188:517–27.

[30] Egan AJ, Rao Y, Viswanathan GB, Smith TM, Ghazisaeidi M, Tin S, Mills MJ. Effect of Nb alloying addition on local phase transformation at microtwin boundaries in nickel-based superalloys. Superalloys 2020:640–50.
[31] Plimpton S. Fast parallel algorithms for short-range molecular dynamics. J Comput Phys 1995;117:1–19.
[32] Mishin Y. Atomistic modeling of the γ and γ′-phases of the Ni-Al system. Acta Mater 2004;52:1451–67.
[33] Amodeo J, Begau C, Bitzek E. Atomistic simulations of compression tests on Ni_3Al nanocubes. Mater Res Lett 2014;2:140–5.
[34] Chen P, Zhang ZW, Liu CS, An T, Yu HP, Qin F. Temperature and grain size dependences of mechanical properties of nanocrystalline copper by molecular dynamics simulation. Model Simul Mater Sci Eng 2019;27:065012.
[35] Shuang F, Aifantis KE. Relating the strength of graphene/metal composites to the graphene orientation and position. Scr Mater 2020;181:70–5.
[36] Shuang F, Dai ZH, Aifantis KE. Strengthening in metal/graphene composites: capturing the transition from interface to precipitate hardening. ACS Appl Mater Interfaces 2021;12:26610–20.
[37] Shuang F, Aifantis KE. A first molecular dynamics study for modeling the microstructure and mechanical behavior of Si nanopillars during lithiation. ACS Appl Mater Interfaces 2021;13:21310–9.
[38] Stukowski A. Visualization and analysis of atomistic simulation data with OVITO-the open visualization tool. Model Simul Mater Sci Eng 2009;18:015012.
[39] Wang YJ, Wang CY. A comparison of the ideal strength between $L1_2$ Co_3(Al, W) and Ni_3Al under tension and shear from first-principles calculations. Appl Phys Lett 2009;94:261909.
[40] Li P, Wang XG, Zhou YZ, Pfetzing-Micklich J, Somsen C, Eggeler G. Effect of aspect ratio on the deformation behavior of dislocation-free Ni_3Al nanocubes. Nanomaterials 2020;10:2230.
[41] Uchic MD, Dimiduk DM, Florando JN, Nix WD. Sample dimensions influence strength and crystal plasticity. Science 2004;305:986–9.
[42] Zuo L, Ngan AHW. Molecular dynamics study on compressive yield strength in Ni_3Al micro-pillars. Philos Mag Lett 2006;861:355–65.
[43] Ngan AHW, Zuo L, Wo PC. Size dependence and stochastic nature of yield strength of micron-sized crystals: a case study on Ni_3Al. Proc R Soc A 2006;462:1661–81.
[44] Zhu T, Li J, Samanta A, Leach A, Gall K. Temperature and strain-rate dependence of surface dislocation nucleation. Phys Rev Lett 2008;100:025502.
[45] Zhu YT, Wu XL. Ductility and plasticity of nanostructured metals: differences and issues. Mater Today Nano 2018;2:15–20.
[46] Shen YF, Lu L, Lu QH, Jin ZH, Lu K. Tensile properties of copper with nano-scale twins. Scr Mater 2005;52:989–94.
[47] Kruml T, Conforto E, Piccolo BL, Caillard D, Martin JL. From dislocation cores to strength and work-hardening: a study of binary Ni_3Al. Acta Mater 2002;50:5091–101.
[48] Wang J, Sehitoglu H. Dislocation slip and twinning in Ni-based $L1_2$ type alloys. Intermetallics 2014;52:20–31.
[49] Liu LL, Wu XZ, Wang R, Li WG, Liu Q. Stacking fault energy, yield strength anomaly, and twinnability of Ni_3Al: a first principles study. Chin Phys B 2015;24:0771023.